Improving surface heat flux estimation for a large lake through model optimization and two-point calibration: The case of Lake Geneva

Abolfazl Irani Rahaghi,[1]* Ulrich Lemmin,[1] Andrea Cimatoribus [ID],[1] Damien Bouffard,[2] Michael Riffler,[3,4] Stefan Wunderle,[3] David Andrew Barry[1]

[1]Faculty of Architecture, Ecological Engineering Laboratory (ECOL), Environmental Engineering Institute (IIE), Civil and Environmental Engineering (ENAC), Ecole Polytechnique Fédérale de Lausanne (EPFL), Lausanne, Switzerland
[2]Faculty of Architecture, Physics of Aquatic Systems Laboratory (APHYS), Margaretha Kamprad Chair, Environmental Engineering Institute (IIE), Civil and Environmental Engineering (ENAC), Ecole Polytechnique Fédérale de Lausanne (EPFL), Lausanne, Switzerland
[3]Faculty of Science, Institute of Geography and Oeschger Centre for Climate Change Research, University of Bern, Bern, Switzerland
[4]Geoville Information Systems GmbH, Innsbruck, Austria

Abstract

Net Surface Heat Flux (SurHF) was estimated from 2008 to 2014 for Lake Geneva (Switzerland/France), using long-term temperature depth profiles at two locations, hourly maps of reanalysis meteorological data from a numerical weather model and lake surface water temperatures from calibrated satellite imagery. Existing formulas for different heat flux components were combined into 54 different total SurHF models. The coefficients in these models were calibrated based on SurHF optimization. Four calibration factors characterizing the incoming long-wave radiation, sensible, and latent heat fluxes were further investigated for the six best performing models. The combination of the modified parameterization of the Brutsaert equation for incoming atmospheric radiation and of similarity theory-based bulk parameterization algorithms for latent and sensible surface heat fluxes provided the most accurate SurHF estimates. When optimized for one lake temperature profile location, SurHF models failed to predict the temperature profile at the other location due to the spatial variability of meteorological parameters between the two locations. Consequently, the optimal SurHF models were calibrated using two profile locations. The results emphasize that even relatively small changes in calibration factors, particularly in the atmospheric emissivity, significantly modify the estimated long-term heat content. The lack of calibration can produce changes in the calculated heat content that are much higher than the observed annual climate change-induced trend. The calibration improved parameterization of bulk transfer coefficients, mainly under low wind regimes.

Surface Heat Flux (SurHF) and wind forcing control stratification dynamics and have a major influence on the physical, chemical, and biological properties of lakes (e.g., MacIntyre et al. 2002; Churchill and Kerfoot 2007; Bonvin et al. 2013; Finlay et al. 2015). For many lakes, changes in heat content are mainly due to SurHF variations, as shown in both short-term investigations (Van Emmerik et al. 2013) and long-term climate change studies (Arvola et al. 2010;

Fink et al. 2014). SurHF temporal variations are often obtained from measurements taken at a single location (e.g., Heikinheimo et al. 1999; Laird and Kristovich 2002; Rouse et al. 2003; Rouse et al. 2008; Nordbo et al. 2011; Van Emmerik et al. 2013; Woolway et al. 2015*a*), using bulk formulas (e.g., Schertzer 1978; Henderson-Sellers 1986; Lenters et al. 2005; Woolway et al. 2015*b*) or 1D numerical modeling (e.g., Tanentzap et al. 2007; Momii and Ito 2008; Austin and Allen 2011; Stepanenko et al. 2014; Thiery et al. 2014*a*; Thiery et al. 2014*b*; Yang et al. 2017). Such quasi one-dimensional (1D) estimates are then considered representative for the whole lake. Although the single-location approach might be suitable for small water bodies, spatial variability of SurHF due to variable meteorological conditions can be important for large lakes (e.g., Lofgren and Zhu 2000; Xue et al. 2015; Moukomla and Blanken 2017). Data from

multiple locations permit the investigation of SurHF spatial variability, and the availability of such data is growing (e.g., Rimmer et al. 2009; Verburg and Antenucci 2010; Spence et al. 2011). A systematic evaluation of the validity and performance of SurHF models at more than one location received little attention up until now, especially for long-term studies. Here, we examine the impact of using data taken at two locations on the bulk SurHF model optimization and calibration and then compare it to the common one-point approach.

An additional source of uncertainty is the selected SurHF model itself. SurHF models involve several terms for the relevant physical processes. For each of these terms, different formulations exist. Some studies aimed to improve and optimize individual SurHF terms (e.g., Fairall et al. 1996; Zeng et al. 1998; Crawford and Duchon 1999; Rimmer et al. 2009; Wang et al. 2014). However, the effect of combining the different equations for all the relevant SurHF terms and optimizing them as a set has not been evaluated.

In this study, we calibrated different combinations of SurHF term equations (with each term describing a different heat exchange mechanism) to quantify the heat content variation of a large lake for a 7-yr period (2008–2014). We also assessed the impact of using time series of temperature profiles taken at two measurement points, instead of at only one point, for the calibration and estimation of SurHF. Lake Geneva, the largest freshwater lake in Western Europe, is a suitable study site as the required data are available. Specifically, the following questions were addressed:

(1) What is the optimal combination of bulk formulas for modeling SurHF in a given lake?

(2) What is the impact of estimating the lake's heat content based on profile data from two measurement locations, as opposed to calibrations based on a single location?

(3) Using the example of Lake Geneva, how sensitive is the lake heat budget variation to the optimal calibration factors in a long-term analysis?

The methodology is developed here using two locations. However, it can be extended to more than two locations. In fact, by increasing the number of locations, it can be expected that the performance of the lake-wide SurHF model will be further improved.

Materials and procedures

Study site

Located between Switzerland and France, Lake Geneva (Local name: *Lac Léman*) is a large, deep perialpine lake with a mean surface altitude of 372 m. It is approximately 70-km long, with a maximum width of 14 km, a surface area of 582 km^2, and a volume of 89 km^3. The lake is composed of two basins: an eastern, large basin called the *Grand Lac*, with a maximum depth of 309 m, and a western, small narrow basin, the *Petit Lac*, with a maximum depth of approximately 70 m (Fig. 1).

The main inflow (*Rhône-in*) and outflow (*Rhône-out*) of the lake are shown in Fig. 1. The lake is surrounded by the Jura Mountains in the northwest, and by the Alps in the south and, to a lesser extent, the northeast (Fig. 1). This topography leads to two dominant wind fields, namely the *Bise* coming from the northeast, and the *Vent* from the southwest (Lemmin and D'Adamo 1996). On average, due to topographic sheltering, the eastern part of the *Grand Lac* experiences lower wind speeds than the western part of the *Grand Lac* and most of the *Petit Lac*. However, the two monitoring locations, SHL2 located in the *Grand Lac* and GE3 in the *Petit Lac* (Fig. 1), for which all the required data for model calibration are available, are located in the part of the lake where the surrounding topography is flat and topographical sheltering effects can be neglected.

Energy balance in a water column

The total heat content of a water column, G_o (Jm^{-2}), is given by:

$$G_o(t) = \int_0^H \rho_w C_{p,w} T(z,t) dz \tag{1}$$

where ρ_w and $C_{p,w}$ are the density (kgm^{-3}) and the specific heat capacity of water at constant pressure (Jkg^{-1} K^{-1}), respectively, and $T[z,t]$ represents vertical temperature profile (°C) at time t down to water column depth $z = H$ (m). The heat content variation from time t_1 to time t_2 then can be quantified by:

$$\Delta G_o(t_1 \rightarrow t_2) = G_o(t_2) - G_o(t_1) \tag{2}$$

The heat content variation in the water column over the full lake depth is the sum of the net energy flux into it and includes net SurHF, Q_N, advective (lateral) heat transport, Q_{ad}, and geothermal heat flux, Q_{ge}:

$$\Delta G_m(t_1 \rightarrow t_2) = \int_{t_1}^{t_2} Q_N(\hat{t}) + Q_{ad}(\hat{t}) + Q_{ge}(\hat{t}) d\hat{t} \tag{3}$$

The contribution of the Q_{ad} and Q_{ge} terms to ΔG_m were compared with that of Q_N. For advective heat transport, note that the measurement locations in this study are far from shore and the river mouth, and that river input effects can be considered to be small, as is evident from the long theoretical residence time of Lake Geneva (11.3 y, Commission Internationale pour la Protection des Eaux du Léman [CIPEL], last accessed 5 July 2018). The contribution of advective heat flux, Q_{ad}, to the heat content variation in the water column, ΔG_m, could be important in lakes with short flushing times due to river inflows (Carmack 1979). In large lakes, the advective heat flux could be significant in certain areas where persistent currents move water between lake regions with different thermal regimes, such as the Keewenaw current in Lake
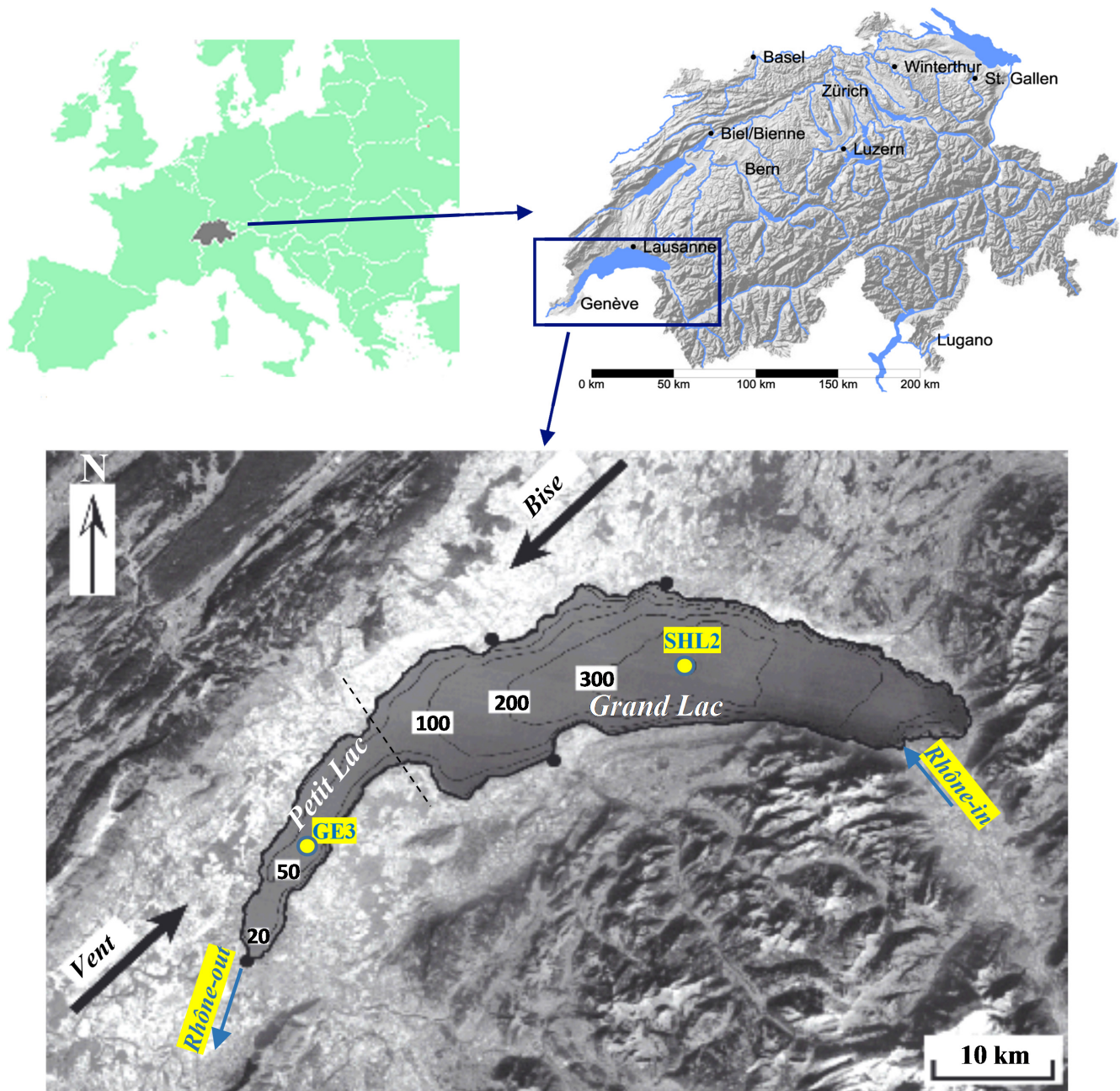
Fig. 1. Location and bathymetry of Lake Geneva, adapted from a public domain satellite image (NASA World Wind, last accessed 5 July 2018) and bathymetry data (SwissTopo, last accessed 5 July 2018). SHL2 (46.45°N, 6.59°E) and GE3 (46.3°N, 6.22°E) are two monitoring locations in the lake used for model calibration and validation. The thick black arrows indicate the direction of the two dominant strong winds over lake called *Bise* and *Vent*. *Rhône-in* and *Rhône-out* show the lake's main river inflow and outflow locations, respectively.

Superior (Zhu et al. 2001), or the bidirectional flow in the Straits of Mackinac (Anderson and Schwab 2017). However, the mean circulation pattern that is most often observed in large lakes is primarily a cyclonic circulation, with well-developed along-shore currents in the near shore zone and mostly weak currents of more random orientation in the central region of the lake (e.g., Emery and Csanady 1973; Simons 1980; Boyce et al. 1989; Beletsky et al. 1999; Beletsky and

Schwab 2008). With this circulation pattern, steady shore-perpendicular currents advecting heat toward the center of the lake are rare. In their numerical modeling of Lake Superior, Bennington et al. (2010) observed that cyclonic circulation dominates and that there is no correlation between the daily anomalies of the local temperature gradient in the meridional direction and the daily anomalies of the current speed in the zonal direction outside the near shore boundary layer. Derecki

(1976) reported that heat advection can be ignored for Lake Erie during most of the year. Based on numerical modeling, a two-gyre (Simons 1980) or three-gyre (Akitomo et al. 2004) large-scale circulation pattern is sometimes found in large lakes.

In the literature, contributions by Q_{ad} and Q_{ge} are ignored and it is assumed that ΔG_m can be approximated by only considering Q_N. To determine whether such a quasi-1D approach is justified in Lake Geneva, we estimated the contribution of Q_{ad} using a three-dimensional (3D) hydrodynamic model. A detailed simulation was performed for a representative period (January to October 2010), as described in the Supporting Information section. The results (Supporting Information Fig. S3) show that far from shore and the main river inflow, the Rhône (Fig. 1), at the locations where this study is carried out, the contribution of SurHF, Q_N, to the heat content variation is much higher than that of lateral advection, Q_{ad}. For the whole lake, the heat content variation due to advective heat flux is high in the near shore zone and low in the center of the lake (Supporting Information Fig. S4), in agreement with Bennington et al. (2010). Thus, in the present analysis, advective heat flux, Q_{ad}, is ignored.

Although the geothermal heat flux, Q_{ge}, is not known for Lake Geneva, it is reported to be small in many Swiss lakes, typically ~ 0.1 Wm^{-2} (Finckh 1976), and its contribution is ignored here. However, we briefly quantify below the impact of this (potential) flux on the estimated parameter values.

The net input energy, ΔG_m (Jm^{-2}), is calculated by integrating the net SurHF, Q_N (Wm^{-2}), for a given period (Eq. 3). The energy balance in the water column can then be written as (Van Emmerik et al. 2013; Fink et al. 2014; Nussboim et al. 2017):

$$\Delta G_o = \Delta G_m \cong \int_{t_1}^{t_2} Q_N(\hat{t}) d\hat{t} \qquad (4)$$

The net heat flux at the air–water interface (positive when directed into the water), Q_N, in Eq. 4 is given by:

$$Q_N = Q_{sn} + Q_{an} + Q_{br} + Q_{ev} + Q_{co} + Q_{pr} \qquad (5)$$

where the right-hand side terms describe the flux due to solar shortwave radiation, Q_{sn}, incoming long-wave radiation from the sky, Q_{an}, back long-wave radiation, Q_{br}, latent (evaporation, Q_{ev}), sensible (convection, Q_{co}), and precipitation (Q_{pr}) heat fluxes. The effect of precipitation, Q_{pr}, on the SurHF of European lakes is neglected due to its minimal influence on SurHF (Livingstone and Imboden 1989; Rimmer et al. 2009; Fink et al. 2014). To use Eqs. 1, 4, and 5, water and atmospheric field data input are required.

Water temperature profiles

CIPEL has measured water temperature profiles ($T(z,t)$ in Eq. 1) since 1957 at locations SHL2 (309 m depth) and GE3 (70 m depth) in the *Grand Lac* and *Petit Lac* (Fig. 1), respectively, at a frequency of 1–2 profiles per month. In total, 130 conductivity-temperature-depth (CTD) profiles at SHL2 and 78 profiles at GE3 are available for the study period (2008–2014). Based on these temperature profiles, the water column heat content variation (Eq. 1) at these two locations was calculated (Supporting Information Fig. S5).

Satellite data

Lake surface water temperatures (LSWTs) are needed for Eq. 5. Riffler et al. (2015) determined the LSWT for 25 lakes in and near the Alps from a long-term archive of Advanced Very High Resolution Radiometer (AVHRR) satellite imagery ($\sim 1.1 \times 1.1$ km pixel size). The satellite-based temperatures agreed well with the near-surface in situ measurements for our study with a bias and root mean square error (RMSE) within the range of -0.5 to $0.6\,°C$ and 1.0 to $1.6\,°C$, respectively. This range of values favorably corresponds with another long-term LSWT calibration for Lake Geneva (Oesch et al. 2005). We use the same data set as Riffler et al. (2015) (4384 images from 1 March 2008 to 31 December 2014) to retrieve the LSWT at the SHL2 and GE3 locations. Images with more than 70% lake coverage were selected, resulting in a total of 856 diurnal images and 308 nocturnal images. Missing pixels in these images were interpolated spatially using Barnes interpolation (Koch et al. 1983; Liston and Elder 2006). The present analysis requires a pixelwise spatially resolved time series of surface temperature. These were derived from the spatially interpolated LSWT maps. Time series were produced using piecewise cubic hermite polynomials (Fritsch and Carlson 1980). Fig. 2a shows the variation of LSWT (labeled T_w in the figures) at the SHL2 and GE3 locations (the nearest pixels in the satellite images) smoothed with a 30-d moving average. Generally, SHL2 has a higher skin temperature than GE3 in summer and winter (Figs. 2a). A shift in the T_w distribution at the two locations is evident from the smoothed probability density function (PDF) of the LSWT (Supporting Information Fig. S6a).

Meteorological data

Meteorological data over Lake Geneva are not measured. However, since 2008, the Swiss Federal Office of Meteorology and Climatology (MeteoSwiss, last accessed 5 July 2018) has run a numerical weather model, COSMO-2, which provides hourly output on a 2.2×2.2 km grid. Lakes are distinguished from land by using a lake model in COSMO-2 (Mironov 2008). COSMO-2 data include spatiotemporal maps of wind speed (10 m above the lake), air temperature (2 m above the lake), relative humidity (2 m above the lake), cloudiness, global radiation and air pressure. Model results are systematically verified against over-land surface data in Switzerland and Europe (MeteoSwiss). This study is based on reanalysis COSMO-2 datasets (assimilated results are based on past field observations) for the period from 1 March 2008 to 31 December 2014. To investigate the quality of COSMO-2
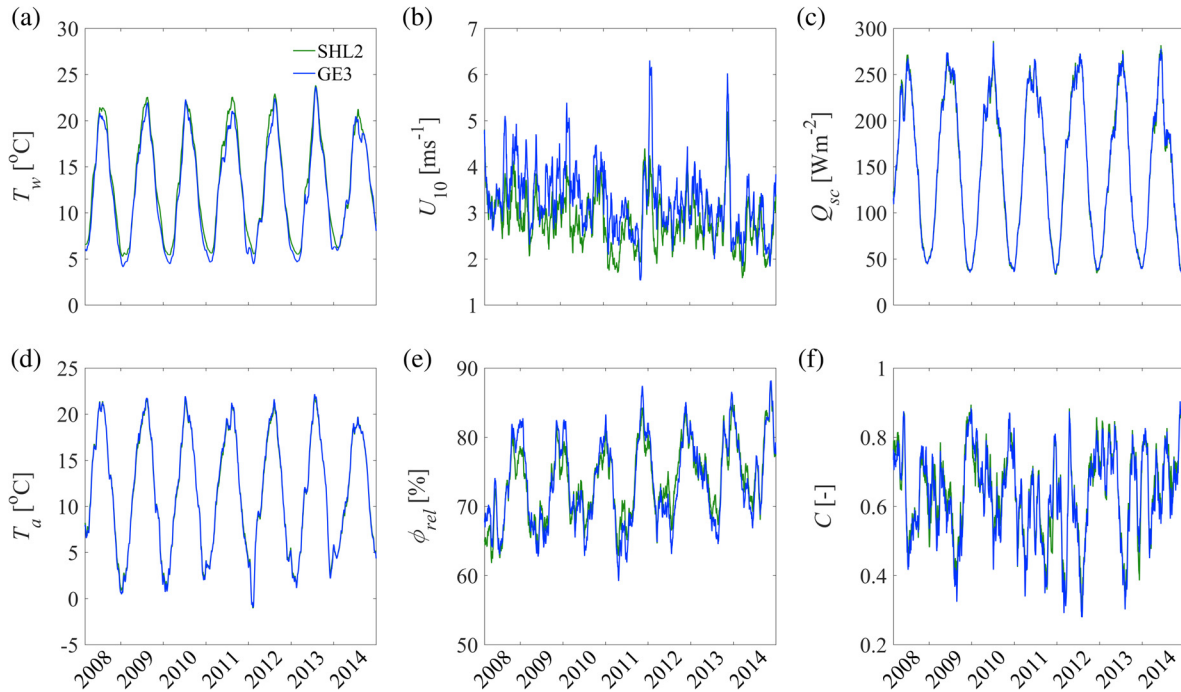
Fig. 2. Time series of LSWT and meteorological data smoothed with a 30-d moving average at SHL2 and GE3 used in the SurHF calculations: **(a)** LSWT, T_w, **(b)** wind speed, U_{10}, **(c)** global radiation, Q_{sc}, **(d)** air temperature, T_a, **(e)** relative humidity, ϕ_{rel}, and **(f)** cloudiness, C.

results further, we compared these data with measurements from meteorological stations located around the lake (Supporting Information Fig. S7a). Our analysis indicates a high correlation between these measurements and the COSMO-2 outputs (Supporting Information Fig. S7b), with the exception of wind speed, which has a higher local spatiotemporal variability. For wind speed, the cross-correlation between different stations is similar for COSMO-2 results and measurements, which confirms the capability of the COSMO-2 model to represent realistic large-scale wind patterns over Lake Geneva (Supporting Information Fig. S7c).

Smoothed meteorological data with a 30-d moving average are shown in Figs. 2b–f, for the SHL2 and GE3 locations (PDFs of the raw hourly data are presented in the Supporting Information S6b–f). The differences between the two locations in variation and distribution of wind speed, U_{10} (Fig. 2b; Supporting Information Fig. S6b), and relative humidity, ϕ_{rel}, (Fig. 2e; Supporting Information Fig. S6e), are pronounced. In particular, the average wind speed is higher at GE3 than at SHL2 (Fig. 2b). The probability density of low wind speeds (1–3 ms^{-1}) is also lower at GE3 (Supporting Information Fig. S6b). This is due to the differences between the characteristics and fetch of the two dominant winds, *Bise* and *Vent*, as described earlier (Fig. 1).

Model calibration procedure

The net SurHF, that is, the air–water heat exchange in Eq. 5, is usually estimated using bulk formulas. These formulas are based on different concepts and require specific

parameters. Ideally, these parameters are known for a given set of conditions (e.g., a lake). However, in reality, this is rarely the case and they have to be determined by calibration.

For each of the five SurHF terms in Eq. 5 that remain to be solved, there are various formulations available in the literature, and their possible combinations give rise to numerous net SurHF models. All of them contain coefficients, which can be a source of error and uncertainty. Model intercomparison is a good way to explore some of the uncertainties and determine the optimal model configuration. In this study, we evaluated 54 net SurHF model combinations and report here in more detail the results for the six combinations considered optimal. Details of the formulas and parameters are presented in the Supporting Information (Tables S1–S4). The model intercomparison indicated that the net SurHF variation, and consequently, the water column heat content are more sensitive to the spatiotemporal variability of atmospheric longwave radiation, Q_{an}, and turbulent heat fluxes, Q_{ev} and Q_{co}, than to the remaining heat flux terms. For Q_{an}, several formulas (e.g., Brutsaert 1975; Satterlund 1979; Crawford and Duchon 1999) with a relatively wide range of values for the corresponding coefficients (*see*, e.g., Supporting Information Table S5,) were reported. Studies over large lakes already indicated a significant spatial variability of turbulent heat fluxes, Q_{ev} and Q_{co}, in particular the latent heat flux, compared to the radiative terms (e.g., Lofgren and Zhu 2000; Verburg and Antenucci 2010; Moukomla and Blanken 2017). There is a similarity between the formulas for the Q_{ev} and Q_{co} estimation that is attributed to the physical analogy between processes

controlling humidity and air temperature. On the other hand, Q_{br} is usually modeled with a constant water surface emissivity value in a relatively narrow range, that is, 0.95–0.97 (Davies et al. 1971; Sweers 1976; Octavio 1977). Thus, for back long-wave radiation, Q_{br}, and also solar short-wave radiation, Q_{sn}, we selected the formulas in the literature reported for previous studies in Switzerland. For the model calibration, therefore, we focused on these three SurHF terms, Q_{an}, Q_{ev}, and Q_{co}. We used one model for Q_{sn} and Q_{br}, two models for Q_{an}, and three models for the Q_{ev}/Q_{co} calculations in Eq. 5.

Table 1 summarizes the references and the corresponding calibration factors for each SurHF component. The combination of equations used in each of the six SurHF models is given in Table 2. It can be seen that any combination requires optimizing four calibration factors. A more complex equation set with additional calibration factors could be imagined. However, in a recent study, Dommenget and Rezny (2018) reported that, in a model tuning problem, a parameter space with higher dimensions will reduce the cost function, but the "modeled physics" are not necessarily closer to the "true physics." Their results indicated that tuning will be more successful by limiting the complexity of the problem to 1–5 calibration factors. Therefore, we calibrated those four parameters for each of the SurHF models, which were found to be most critical in our preliminary 54 model intercomparison.

The calibration factors listed in Table 1 were optimized based on energy conservation over time (Eq. 4). The generalized likelihood uncertainty estimation (GLUE) methodology (Beven and Binley 1992) was applied to calibrate the six SurHF models in Table 2. This methodology requires a validity range for each parameter, a sampling strategy for the parameter space and a likelihood measure for each parameter set. The range of different parameters was chosen according to physical limitations and their reported ranges in the literature, particularly for Swiss lakes. The details on the range of parameters and the sampling strategy can be found in the Supporting Information. To evaluate the temporal variation of the model

heat content, the RMSE with respect to observations was selected as the minimized optimization metric:

$$RMSE = \sqrt{\frac{\sum_{i=1}^{N}\{[G_o(t_i)-G_o(t_1)]-[G_m(t_i)-G_m(t_1)]\}^2}{N}} \tag{6}$$

where N is the number of total observations at the two measurement locations (SHL2 and GE3, Fig. 1) at time t_i. However, in cases where RMSEs are close for different models, other metrics, such as correlation coefficient and standard deviation were used.

The approach used here is based on the optimization of Q_N by minimizing the uncertainties with respect to the observed water column heat content G_o. However, Q_N is the sum of different SurHF components and minimizing the uncertainty of the sum may create erroneous values of the individual terms, which may cancel each other. To determine the errors in the estimates of each SurHF component, direct measurements of each component are required. These errors cannot be estimated in the present study, because such data are not available for Lake Geneva. Instead, we will further investigate this point below by examining the dynamics of the individual components and compare their values with those reported in the literature.

Table 2. Equations used in each of the six selected SurHF models. *See* Table 1 for references for each heat flux term (details are given in the Supporting Information Tables S1–S4).

Model number	Constituent equations
1	$Q_{sn} + Q_{an1} + Q_{br} + (Q_{ev} + Q_{co})_1$
2	$Q_{sn} + Q_{an1} + Q_{br} + (Q_{ev} + Q_{co})_2$
3	$Q_{sn} + Q_{an1} + Q_{br} + (Q_{ev} + Q_{co})_3$
4	$Q_{sn} + Q_{an2} + Q_{br} + (Q_{ev} + Q_{co})_1$
5	$Q_{sn} + Q_{an2} + Q_{br} + (Q_{ev} + Q_{co})_2$
6	$Q_{sn} + Q_{an2} + Q_{br} + (Q_{ev} + Q_{co})_3$

Table 1. Selected bulk formulas and their corresponding calibration coefficients for five SurHF components (details of each model are given in the Supporting Information Tables S1–S4).

SurHF components and equations			References	Corresponding calibration factors
Solar shortwave radiation	Q_{sn}	Supporting Information Eq. S1	Cogley (1979); Fink et al. (2014)	-
Atmospheric long-wave radiation	Q_{an1}	Supporting Information Eq. S2	Brutsaert (1975)	C_{an} and C_{cloud}
	Q_{an2}	Supporting Information Eq. S3	Crawford and Duchon (1999)	C_{lc} and C_{lt}
Back radiation	Q_{br}	Supporting Information Eq. S4	Livingstone and Imboden (1989); Fink et al. (2014)	-
Latent (evaporation) and sensible (convection) heat fluxes	$(Q_{ev} + Q_{co})_1$	Supporting Information Eq. S5	Bowen (1926); Murakami et al. (1985)	C_{mur} and C_b
	$(Q_{ev} + Q_{co})_2$	Supporting Information Eq. S6	Ryan et al. (1974); Gill (1982)	$C_{e,r}$ and $C_{h,r}$
	$(Q_{ev} + Q_{co})_3$	Supporting Information Eq. S7	Monin and Obukhov (1954); Woolway et al. (2015b)	C_{m2} and C_{q1}

Another source of error in RMSE calculations (Eq. 6) is the uncertainty of the measured temperature profiles used to calculate G_o. In the Error analysis in the Supporting Information, we estimate this error and it will be demonstrated below that it is much smaller than the smallest RMSE values. Thus, RMSEs essentially report errors in G_m.

Assessment and results

Model calibration and assessment

Uncalibrated versus calibrated net surface heat flux models

Various combinations of SurHF models were studied applying the water column energy balance First, we examined the performance of the different models using coefficient values given in the literature, with an emphasis on those used in other lake studies in Switzerland. These include $C_{cloud} = 0.17$, $C_{an} = 1.0592$, and $C_b = 0.62$ as in the study by Fink et al. (2014), $C_{lt} = 0.06$ and $C_{lc} = 1.22$ (Crawford and Duchon 1999), $C_{mur} = 1.2 \times 10^{-7}$ (Murakami et al. 1985), $C_{e,r} = 2.1 \times 10^{-3}$ and $C_{h,r} = 1.45 \times 10^{-3}$ (Wahl and Peeters 2014), $C_{m2} = 0.11$ and $C_{q1} = -2.67$ (Zeng et al. 1998).

A Taylor diagram (Taylor 2001) was used to determine how well the results of the six SHF models matched the observations (Eq. 4). The Taylor diagram (Fig. 3) provides a comparison between a group of models and a reference observation by combining correlation coefficients, RMSE and standard deviations in a single figure. Here, the reference is the heat content variation at the SHL2 and GE3 locations, ΔG_o, calculated by Eqs. 1 and 2. The comparison groups are the heat content variation calculated with these six different net SurHF models, ΔG_m, estimated by Eq. 3. These models and their corresponding SurHF terms are described in Tables 1 and 2. The results reveal that the models using the predefined (uncalibrated) values lead to a high standard deviation and RMSE (1.2–7.7 GJm^{-2}), and a low correlation coefficient (less than 0.4) compared to the observations. These substantial deviations emphasize the importance of performing a pre-analysis before applying the SurHF models for long-term air-water heat exchange investigations. For example, model results indicate that employing predefined calibration factors results in nonphysical atmospheric emissivity values $\varepsilon_{an} > 1$ and consequently significant model-observation divergence. The model-observation deviation is higher for uncalibrated models using atmospheric emissivity as proposed by Crawford and Duchon (1999), ε_{an2} (Supporting Information Eq. S3b, Table S1), resulting from an overestimation of Q_{an2} due to a presumably high (uncalibrated) C_{lc} value, 1.22. Crawford and Duchon (1999) reported a monthly mean bias error of −9 to 4 Wm^{-2} based on their data for a 1-yr period using this formula. In summary, all six models using these predefined coefficients failed to reproduce the heat content variation at both the SHL2 and GE3 locations.
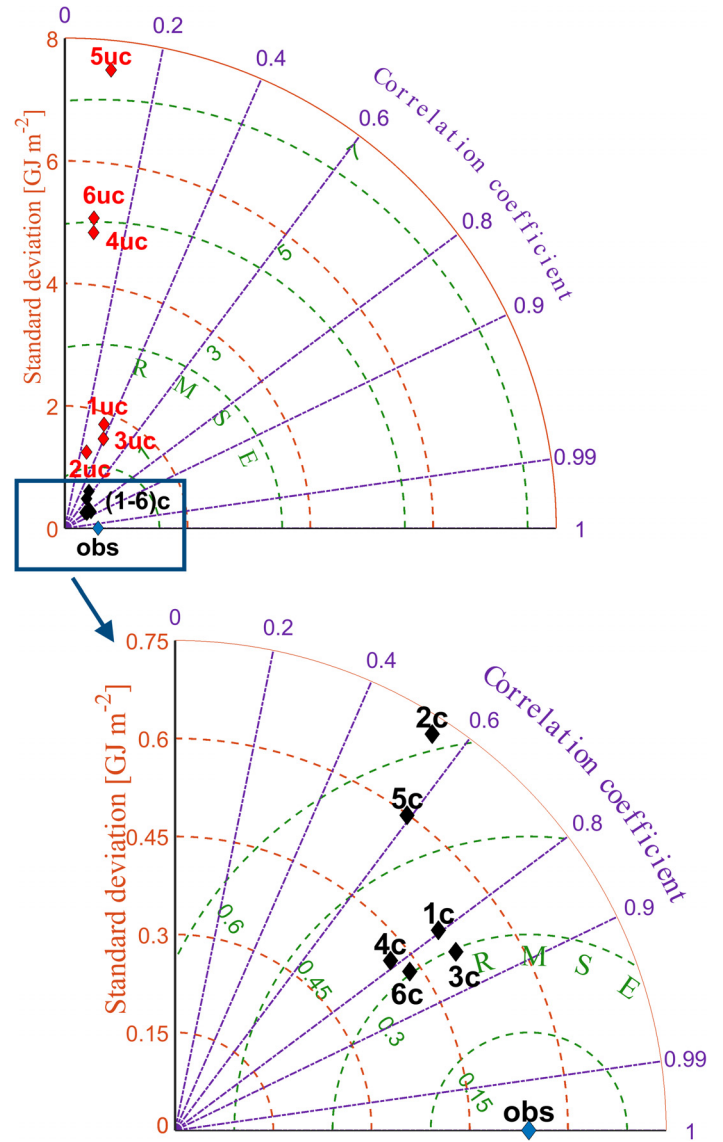

Fig. 3. Taylor diagrams showing a statistical comparison of the individual net surface heat flux (SurHF) models with respect to observations. Both uncalibrated, "uc" (in red), and calibrated, "c" (in black), models are shown by their corresponding numbers (Table 2). Green dashed lines, orange dashed lines, and purple dashed lines indicate RMSE, standard deviation, and correlation coefficient, respectively. The lower diagram is a zoom of the blue rectangle in the upper diagram. For details, see the text.

Therefore, we followed the optimization and calibration procedure for all model combinations, as explained above, using a two-location calibration approach. The zoomed lower panel of Fig. 3 presents the model-observation comparison for the optimum (calibrated) net SurHF models and the combined observations at SHL2 and GE3. The results show a great improvement over the uncalibrated estimations. Models 1 and 4 (Table 2), which calculate turbulent heat fluxes using $(Q_{ev} + Q_{co})_1$ have a higher correlation coefficient, lower RMSE and smaller standard deviation than Models 2 and 5 using $(Q_{ev} + Q_{co})_2$. The simple

Murikami's and Bowen's formulations, $(Q_{ev} + Q_{co})_1$, yield a better estimation of Lake Geneva's surface heat exchange than considering the effect of both free and forced convection in $(Q_{ev} + Q_{co})_2$. For the model of Ryan et al. (1974), turbulent heat fluxes, $(Q_{ev} + Q_{co})_2$, were derived under laboratory conditions where forced convection is not significant compared to free convection and the air–water temperature difference was greater than in natural systems. However, the similarity theory, $(Q_{ev} + Q_{co})_3$ in Table 1, applied in Models 3 and 6, reproduces the temporal variation of turbulent heat fluxes far better than the other two algorithms. This model, $(Q_{ev} + Q_{co})_3$, iteratively determines the atmospheric boundary layer condition at each point and at each time step based on the LSWT and meteorological data, and better resolves the spatial variability of SurHF. Results indicate that for approximately 75% of the time, the atmospheric boundary layer over the lake is unstable.

Since the calibrated Models 3 and 6 have similar RMSEs, we applied additional statistical methods, i.e., correlation coefficient and standard deviation, to select the best model for SurHF estimation. We also calculated the bias between the observed and modeled heat contents for each model. These two models have nearly identical correlation coefficients and RMSEs (purple lines and green lines in Fig. 3). However, Model 3 gives a slightly better standard deviation than Model 6 (orange lines in Fig. 3) while the estimated bias using Model 6 is slightly smaller than Model 3. Although the temporal variation of heat contents by implementing Model 3 and Model 6 are not noticeably different (results not shown), Model 3 was selected as the best model resulting from the Taylor diagram comparison (Fig. 3).

Two-point versus one-point calibration

Our analysis (Fig. 3) shows that, regardless of the chosen model, recalibration greatly improves the estimation of the long-term surface heat exchange for Lake Geneva. In order to determine whether there is a significant difference between the one-point and two-point calibration, we calibrated the six SurHF models using either SHL2 or GE3 temperature profiles. Fig. 4 shows the heat content variation comparison between observations ΔG_o and Model 3 results ΔG_m. The SurHF model calibrated at SHL2 overestimates the SurHF at GE3 (Fig. 4a), while SurHF values are underestimated at SHL2 using only GE3 temperature profiles for model calibration (Fig. 4b). Therefore, SurHF models calibrated using only one temperature profile location fail to predict the profile at the other location. Similar results were obtained using the other five net SurHF models (results not shown). This confirms that there is a significant difference between the one-point and two-point calibration.

Intercomparison of lake heat content variation

A group of four optimal calibration factors was obtained for each of the six models, listed in Table 2, using the two-point calibration. For the remaining analysis, only these optimal values are employed. The observed heat content variation,

ΔG_o, and the corresponding heat content variation using the six different calibrated models, ΔG_m, are compared in Fig. 5. Here, the individual model performances at SHL2 and GE3 are investigated separately. Using Models 2 and 5, the SHL2 and GE3 results are roughly distributed below and above the optimal dashed line, respectively, and have the largest scatter. This demonstrates that the worst combination of sensible-latent heat flux terms $(Q_{ev} + Q_{co})_2$ (Supporting Information Eq. S6, Table S3), underestimates the SurHF at SHL2, while it is overestimated at GE3. Although this two-point separation is less pronounced using Models 1 and 4 (left panels of Fig. 5), these models still have a relatively higher RMSE and lower correlation coefficient compared to the best models (Fig. 3). Models 3 and 6, which are the best models in terms of RMSE, use similarity theory $(Q_{ev} + Q_{co})_3$ (Supporting Information Eq. S7, Table S3), for turbulent heat flux estimation. Model 3 uses Brutsaert's formulation (Supporting Information Eq. S2, Table S1), while Crawford-Duchon's approach (Supporting Information Eq. S3, Table S1) quantifies atmospheric radiation in Model 6. Therefore, using a more advanced model for the sensible-latent SurHF calculation, Supporting Information Eq. S7, Table S3, not only it leads to better model-observation statistics but also reproduces the heat content of individual points better than the other models.

When comparing Models 1–3 (top panels) with Models 4–6 (bottom panels) in Fig. 5, it should be noted that in the top panels, the results for SHL2 mainly cluster above the optimal line, whereas those for GE3 are mainly below that line. Such a clear separation between the results of the two stations is less obvious in the bottom panels. Models 1–3 apply the Brutsaert (1975) formulation for cloud cover, and the remaining models use the more complex model of Crawford and Duchon (1999). This latter formulation gives more realistic results in terms of the model bias.

Using the best and worst models (respectively, Model 3, closest to "obs" in Fig. 3, and Model 2, furthest from "obs" in Fig. 3), time series of the modeled lake heat content at the calibration locations are compared with observations in Fig. 6. As stated earlier, the calibration factors are assumed constant. However, if each location is treated independently in the calibration process, with a different set of calibration parameters for each model at each of the two stations, there is little or no difference between the models (results not shown). This, again, demonstrates the significant improvement resulting from the two-point calibration and the use of optimal heat flux term concepts. The failure of some models, for example, Model 2, to resolve the spatial variability of heat content, that is, two-point calibration in this study, could be due to incorrectly modeling some relevant physical processes or not modeling them at all. As the long-wave radiation Q_{an} shows little spatial variability over the lake, the turbulent heat flux model $(Q_{ev} + Q_{co})_2$ (Table 2) can be considered the source of the deviation of Model 2. It was already shown earlier (Figs. 3 and 5) that Model 2 significantly differs from the observations.
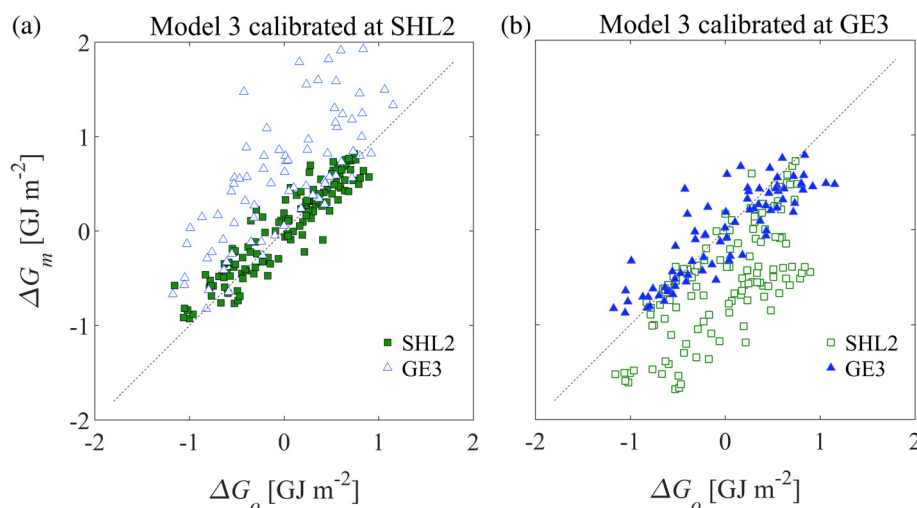
Fig. 4. Heat content variation comparison between observations at SHL2 (green squares) and GE3 (blue triangles) employing Model 3 with a calibration at **(a)** SHL2, and **(b)** GE3.
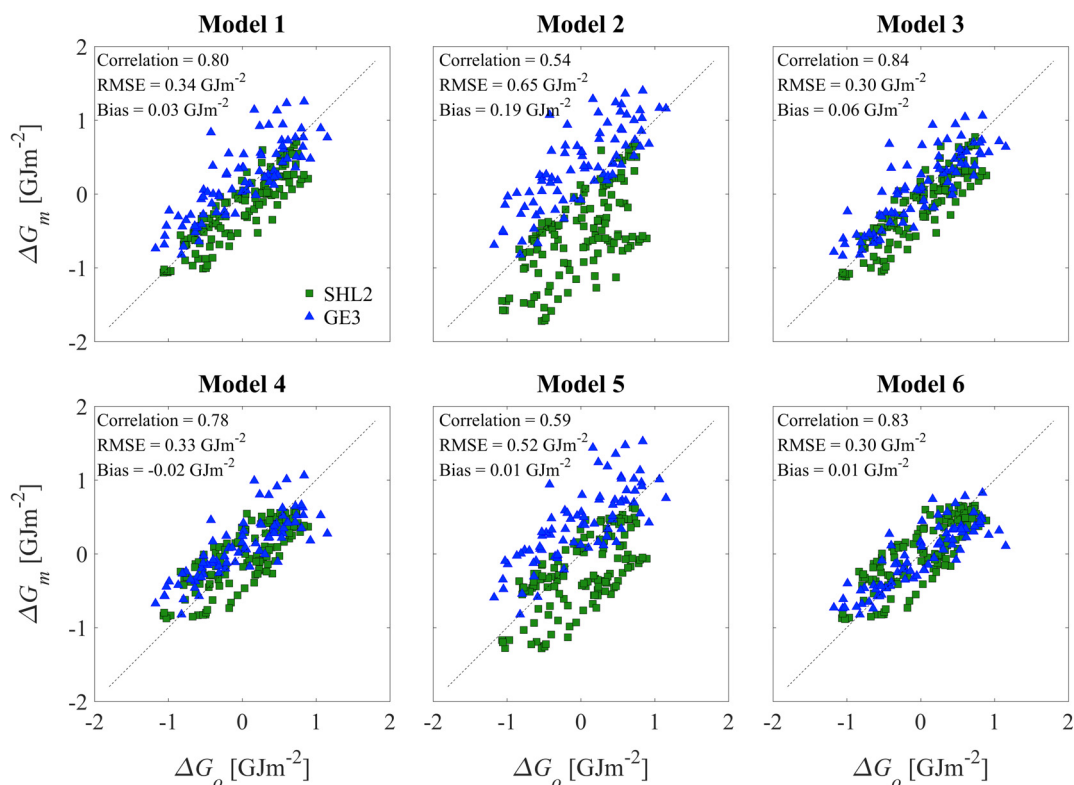

Fig. 5. Heat content variation comparison between observations at SHL2 (green squares) and GE3 (blue triangles) for six different model combinations. The individual formulas used in each model are given in Table 2 (*see* Supporting Information Tables S1–S4 for more details).

Intercomparison of net surface heat flux

In order to compare the net SurHF, Q_N (Wm^{-2}), at SHL2 and GE3 obtained with the six selected models using the best-fit parameters, the mean and standard deviation of Q_N were calculated for the period 1 Jan 2009 to 31 Dec 2014 (due to missing data, the January–February 2008 results were excluded). The mean value of SurHF at GE3 is higher than at SHL2 in all models (Table 3). The mean SurHF difference ranges from 4 to 10.7 Wm^{-2} for Models 6 and 2, respectively. In terms of mean net SurHF, Model 6, and to a lesser extent Model 1, are close to Model 3, while Model 2 has the largest deviation. The results of Models 5 and 6 have the maximum and minimum standard deviation differences with respect to Model 3 at the two locations. Consequently, there will be
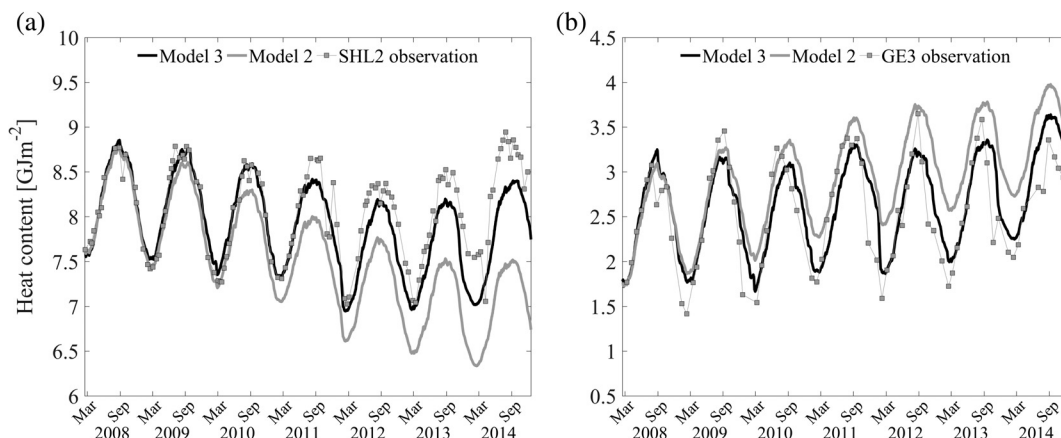
Fig. 6. Temporal evolution of the lake heat content. Model results compared to observations (points) at **(a)** SHL2, and **(b)** GE3 (*see* Fig. 1 for station location). Only the best (Model 3, black lines) and the worst (Model 2, gray lines) models are presented. Note that due to the difference in depth at the two locations, that is, 309 m at SHL2 and 70 m at GE3, the absolute values of heat content (vertical axis) have different magnitudes in **(a)** and **(b)**.

Table 3. Mean and standard deviation of net SurHF, Q_N, at SHL2 and GE3 using the six SurHF models specified in Table 2 for the period 2009–2014. Model 3, in bold, is the best model based on the results in the Taylor diagram (Figs. 3 and 5).

		Model 1	Model 2	Model 3	Model 4	Model 5	Model 6
Mean (Wm^{-2})	SHL2	−1.1	−6.2	**−1.0**	0.4	−2.5	−0.7
	GE3	4.7	4.5	**3.4**	4. 8	6.1	3.3
Standard deviation (Wm^{-2})	SHL2	221.9	219.4	**232.4**	219. 6	219.4	228.6
	GE3	223.2	220.2	**238.9**	222.2	219.6	235.8

marked differences between the models if integrated over the entire lake and considered over an annual cycle.

The mean net SurHF at SHL2 and GE3 are −1 and 3.4 Wm^{-2}, respectively, for 2009–2014. The results also indicate that on average, some parts of the lake (GE3) are warming at the same time as other regions (SHL2) are cooling down during this period. This emphasizes the importance of using multiple locations (or ideally the entire lake) instead of only one location for SurHF and lake heat content studies, especially for long-term analyses. The high standard deviation values in Table 3 result from using hourly estimates. When the data are smoothed with a 30-d moving average, standard deviations of 88.9 and 95.6 Wm^{-2} for SHL2 and GE3, respectively, are obtained with Model 3. Although the difference between these standard deviations is small, it shows that the SurHF distribution can vary systematically from one point to another over a large lake. Furthermore, the SurHF values are spread over a wider range at GE3 than at SHL2. This distribution is the response to the combined contribution of various meteorological parameters, for which spatial variations are likely to occur. Fig. 2; Supporting Information Fig. S3, for example, illustrate this variability at the two studied locations.

Surface heat flux estimation

We calculated SurHF terms at two locations using the best model (Model 3), with the following four optimal coefficient values: $C_{\text{cloud,opt}} = 0.11$, $C_{\text{an,opt}} = 0.98$, $C_{m2,\text{opt}} = 0.01$, and $C_{q1,\text{opt}} = -1.52$. The results converge to a minimum RSME value

for all four parameters with a narrow range of variation in the neighborhood of these optimal parameter values (Supporting Information Fig. S9). Furthermore, the uncertainty analysis also showed a negligible error of the observation data, G_o, compared to the above minimum RMSE value (*see* error analysis in the Supporting Information). The $C_{\text{cloud,opt}}$ value we obtained ($C_{\text{cloud,opt}} = 0.11$) is lower than $C_{\text{cloud}} = 0.17$ determined by Kuhn (1978) and used in other studies in Switzerland (Livingstone and Imboden 1989; Fink et al. 2014). Our parameter $C_{\text{an,opt}}$ ($C_{\text{an,opt}} = 0.98$) is also slightly lower than the values of 1.09 and 1.0592 used in those studies. To verify the calibrated values for C_{cloud} and C_{an}, we evaluated the computed atmospheric emissivity for the SHL2 and GE3 stations. The emissivity values, ε_{an1} (Supporting Information Eq. S2b, Table S1), fluctuate between 0.6 and 1, with the lower emissivity values being valid for clear skies and low air temperatures in winter and the highest values during warm and fully cloudy summertime conditions (Supporting Information Fig. S10). This shows the improvement resulting from our calibration for this SurHF component, as it was previously mentioned that uncalibrated emissivity may reach values >1 which are physically unrealistic. The C_{m2} and C_{q1} factors will be further discussed in the next section.

The calculated temporal variation of the five SurHF terms and the net SurHF for the study period using Model 3 is presented in Fig. 7 (smoothed with a 30-d moving average). There is a high correlation (>0.97) for the radiative heat fluxes, Q_{sn}, Q_{an}, and Q_{br} at SHL2 and GE3. However, due to the difference in variation of
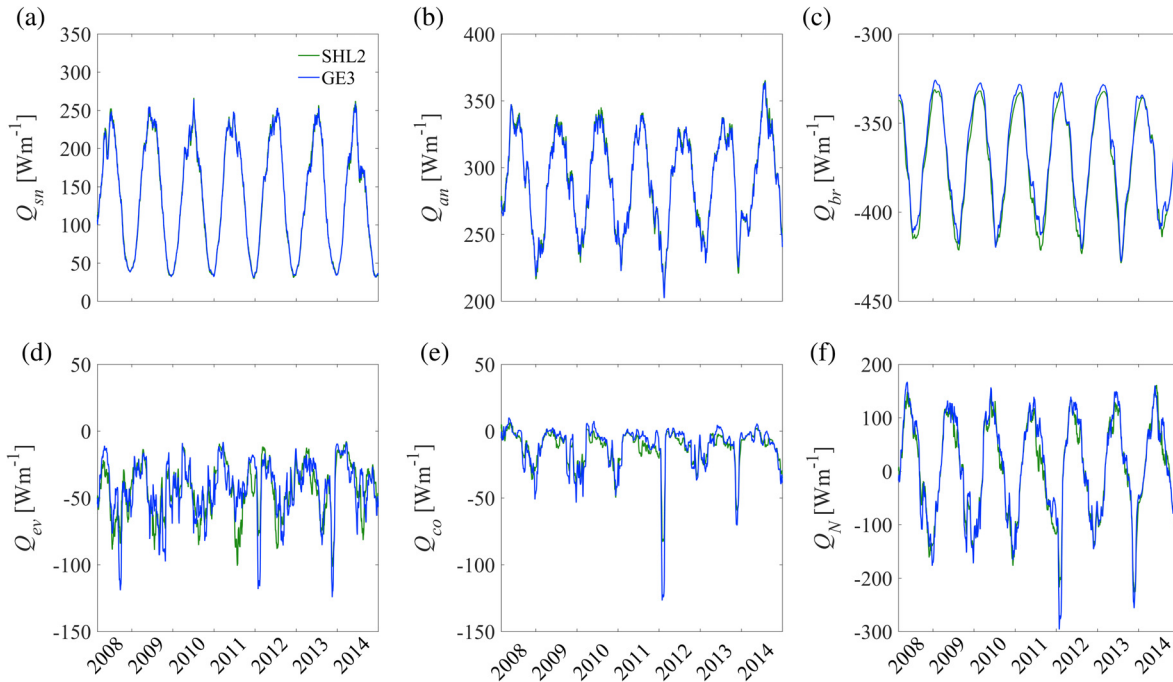
Fig. 7. Long-term time series of the surface heat flux (SurHF) terms and net SurHF of Lake Geneva at SHL2 (green lines) and GE3 (blue lines) smoothed with a 30-d moving average obtained with model 3: **(a)** solar radiation, Q_{sn}, **(b)** atmospheric radiation, Q_{an}, **(c)** back radiation, Q_{br}, **(d)** latent heat flux, Q_{ev}, **(e)** sensible heat flux, Q_{co}, and **(f)** net SurHF, Q_N. The horizontal axis indicates the year.

Table 4. Mean and standard deviation of different SurHF terms at SHL2 and GE3 using Model 3 for the period of 2009–2014.

	Location	Q_{sn}	Q_{an}	Q_{br}	Q_{ev}	Q_{co}
Mean (Wm^{-2})	SHL2	136.4	289.7	−371.4	−42.8	−12.9
	GE3	137.2	288.7	−367.5	−42.7	−12.3
Standard deviation (Wm^{-2})	SHL2	210.4	50.6	30.8	58.4	31.1
	GE3	210.7	50.2	30.6	64.7	39.8

wind speed, relative humidity and LSWT at SHL2 and GE3 (U_{10}, ϕ_{rel} and T_w in Fig. 2; Supporting Information Fig. S6), the correlation coefficients of sensible, Q_{co}, and latent, Q_{ev}, heat fluxes between SHL2 and GE3 are 0.8 and 0.63, respectively, based on hourly values. A correlation coefficient of 0.93 was found between the net SurHF Q_N at SHL2 and GE3. The mean and standard deviation of the different SurHF terms at both locations for the period 1 Jan 2009 to 31 Dec 2014 are given in Table 4. Examining the results for different SurHF terms reveals that radiative components mainly contribute to the variation of the mean net SurHF at each location. The higher standard deviation of the net SurHF at the GE3 location compared to SHL2 (Table 3) can be explained by the higher standard deviation values of turbulent heat fluxes at this location (Table 4).

Discussion

Bulk transfer coefficients

The model assessment shows that using an appropriate model for the sensible-latent heat flux estimation is essential for the two-point calibration. The results indicate that some models fail to reflect the long-term heat content variation at two points. Based on the RSME, the bulk aerodynamic algorithm using the similarity theory and empirical relationships $(Q_{ev} + Q_{co})_3$ in Table 2 (details in the Supporting Information Eq. S7, Table S3), was the best model. Two components must be defined in this algorithm: turbulence stability functions, f_m, f_e, and f_h, and roughness lengths for momentum, temperature and humidity, z_0, z_{0t}, and z_{0q}, respectively. Details of the calculation procedure are given in the Supporting Information. Unlike the other selected models, that is $(Q_{ev} + Q_{co})_1$ and $(Q_{ev} + Q_{co})_2$ in Table 2, the heat transfer coefficients are not constant in this algorithm. The spatiotemporal values of the transfer coefficients, $C_{d,m}$, $C_{e,m}$, and $C_{h,m}$, are defined as a function of the atmospheric stability parameter (ζ, Supporting Information Eq. S7e, Table S3) using the Monin-Obukhov theory (Monin and Obukhov 1954). Even though wind speed is often considered to be the main physical parameter affecting the transfer coefficient values, other processes such as air thermal stratification (e.g., Deardorff 1968; Xiao et al. 2013),

waves and relative humidity may also contribute (Toffoli et al. 2012). The transfer coefficients are higher under unstable atmospheric boundary layer conditions. However, the effect of humidity and wave parameters on the air-water heat and momentum exchanges was found to be different under weak and strong wind conditions. In order to include these processes in the calibration procedure, field measurements are needed which are not available for Lake Geneva.

The obtained optimal values, $C_{m2,opt} = 0.01$ and $C_{q1,opt} = -1.52$, are, respectively, lower and higher than the optimum values of Zeng et al. (1998), that is, $C_{m2,uc} = 0.11$ and $C_{q1,uc} = -2.57$. Fig. 8 illustrates the variation of $C_{e,m}$ and $C_{d,m}$ as a function of wind speed, U_{10}, when the uncalibrated and calibrated factors are compared. The coefficient $C_{h,m}$ has a similar shape as $C_{e,m}$ (not shown). These curves were obtained by randomly sampling 2000 points from the dataset under unstable conditions (negative stability parameter, $\zeta < 0$). Following the sensitivity analysis in the Supporting Information Fig. S8, the difference between calibrated and uncalibrated factors results in lower (higher) humidity and temperature bulk transfer coefficients under low (high) wind speed conditions (Fig. 8a). We assumed a constant value of 0.013 for the Charnock parameter (Charnock 1955) in the calculation of the momentum roughness length, z_0 (Supporting Information Eq. S10). Therefore, the drag coefficient, $C_{d,m}$ under high wind conditions (> 7 ms^{-1}) is similar for uncalibrated and calibrated conditions (Fig. 8b).

To verify the calibration factors, we compare the shape and range of these curves with some measurements taken over water. The general form of theses curves is similar to the measured values over inland and open waters (e.g., Wüest and Lorke 2003; Wei et al. 2016). As we obtained lower values for both C_{m2} and C_{q1} than Zeng et al. (1998), the calibrated transport coefficients are smaller (higher) at low (high) winds than the uncalibrated coefficients in Fig. 8. These coefficients are

sensitive to the choice of parameterization, especially in low wind regimes (Webster and Lukas 1992). For weak winds, the measured data cover a wide range of drag coefficients from ~2 × 10^{-3} to 2 × 10^{-2}. Higher coefficient values (~2 × 10^{-2}) are reported mainly for ocean experiments (Geernaert et al. 1988; Bradley et al. 1991) while lower values (~2 × 10^{-3}) were observed over shallow coastal waters (Mahrt et al. 1996) and estuaries (Lin et al. 2002). Wei et al. (2016) found a high drag coefficient value of ~10^{-2} at a wind speed of ~1 ms^{-1} for Lake Kasumigaura (Japan), while a value of ~2.5 × 10^{-3} was measured for Lake Neuchatel (Switzerland) for the same wind speed (Simon 1997). For Lake Kasumigaura, however, the humidity transfer coefficient was ~3 × 10^{-3} at 1 ms^{-1} wind speed, which is closer to our estimated values (Fig. 8a). Under high wind regimes, the calibrated value (~2 × 10^{-3}) and the almost linear variation of the transfer coefficients are in agreement with reported measurements (Graf and Prost 1980; Merzi and Graf 1988; Mahrt et al. 1996; Babanin and Makin 2008; Toffoli et al. 2012; Wei et al. 2016). Although the transfer coefficient values are consistent with other studies, there is a shift in the wind speed under which these minima are observed. The minimum values of the transfer coefficients (~10^{-3}) were obtained at a low wind speed of ~2 ms^{-1} (Fig. 8), whereas the minima reported in the literature are, for example, at ~4 ms^{-1} (Mahrt et al. 1996; Lin et al. 2002) or ~5 ms^{-1} (Wüest and Lorke 2003; Wei et al. 2016).

The large scatter seen in the transport coefficients under weak wind regimes could be due to the measurement technique, method of statistical calculation, or site-dependent parameters. Recently, Wei et al. (2016) suggested some possible reasons for high values at low wind speeds, for example, lake surface currents, wave effects, and gustiness. However, the behavior of transfer coefficients under low wind speeds is less clear. Mahrt et al. (1996) investigated the influence of fetch on the drag coefficient curve. They reasoned that the
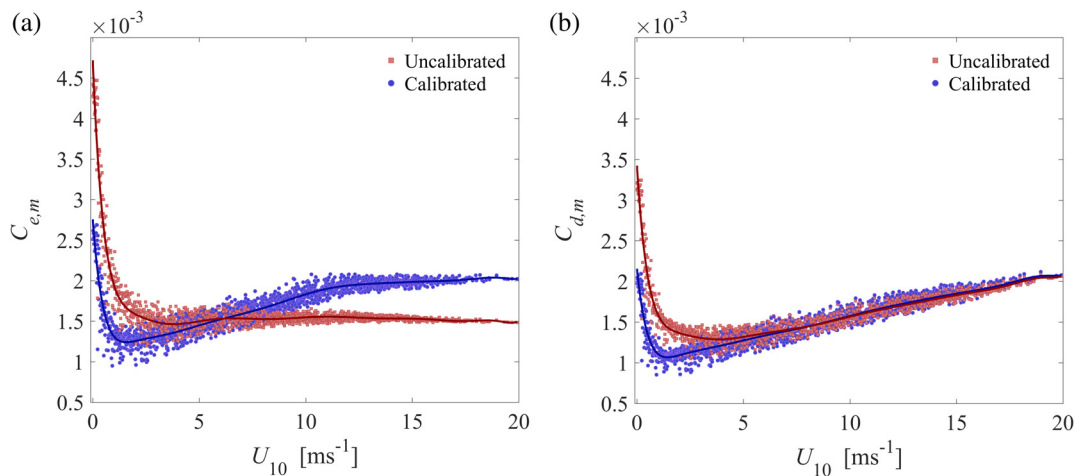

Fig. 8. (a) Humidity bulk transfer coefficient, $C_{e,m}$, and **(b)** drag coefficient, $C_{d,m}$, as a function of wind speed, U_{10}, using uncalibrated ($C_{m2,uc} = 0.11$ and $C_{q1,uc} = -2.57$; in red) and calibrated parameters ($C_{m2,opt} = 0.01$ and $C_{q1,opt} = -1.52$; in blue).

drag coefficient for a short fetch (<4 km) is greater than for a long fetch, particularly for high wind speeds. They associated this variation to the wave field difference under different fetches. Their results also indicate that the drag coefficient for short fetches has a minimum at a wind speed of ~3 ms^{-1}. Our results agree with the short-fetch results of Mahrt et al. (1996), especially for low wind speeds (< 3 ms^{-1}). The variation of transport coefficients in this regime is mainly due to the second term in the right-hand side of the Supporting Information Eq. S10, $C_{m2}v_a/u_*$. Compared to measurements by Zeng et al. (1998), Wüest and Lorke (2003), and Wei et al. (2016), the lower transport coefficients at low wind speeds reported here are due to the small C_{m2} value, 0.01, compared to the commonly used value of 0.11. Other parameterizations for this term are proposed, for example, $C_{m3}\sigma_w/\rho_w u_*^2$ (Jin 1994; Bourassa et al. 1999), where C_{m3} is a calibration factor and σ_w is the surface tension. Better insight into realistic parameterizations could be obtained from systematic direct measurements of the atmospheric boundary layer.

Sensitivity of the calibration factors

We quantified the effect of uncertainty associated with the four calibration factors using a straightforward sensitivity analysis in which one parameter was varied over a specific range while keeping the remaining three constant. The difference in heating/cooling caused by the different parameters is expressed as the temperature change in the near surface water layer, for example, the upper 10 m of the water column, ΔT (°Cy^{-1}), using:

$$\Delta T = \frac{\Delta G_{m,\text{sen}}}{\rho_w C_{p,w} H_{sl}} \qquad (7)$$

where $\Delta G_{m,\text{sen}}$ (Jm^{-2}y^{-1}) is the mean annual heat content change due to variation of the corresponding parameter, and H_{sl} is the surface layer depth (m). This metric was used to compare the cooling/heating induced by employing uncalibrated SurHF box models with a warming water temperature trend. In this context, a ± 1°Cy^{-1} variation is approximately equal to a ± 1.3 Wm^{-2} bias in the estimation of the net SurHF.

Fig. 9 shows the effect on the heat content variation at SHL2 and GE3. The results indicate that relatively small deviations in calibration factors, particularly in C_{an}, affect the lake's temperature trend significantly and can be much higher than the annual climate change trend of 0.065°Cy^{-1} as reported by Gillet and Quetin (2006) for the near surface layer. Variations in C_{an} and C_{cloud} have a linear influence on the heat flux estimation (Figs. 9a,b) while the effect of an uncalibrated C_{q1} and C_{m2} is non-linear (Figs. 9c,d). This is due to nonlinearity inherent in the turbulent heat flux parameterization. The sensitivity of the results to C_{an} variations is striking (Fig. 9a), whereas variations of C_{q1} are less marked (Fig. 9c). A small deviation in C_{an} (< 1%) results in a noticeable change in the SurHF estimation (> 2.5 Wm^{-2}) and consequently the lake heat content.

The results are also sensitive to C_{cloud}. A ± 10% variation of C_{cloud} leads to a bias of ~ ±1.6 Wm^{-2} in the estimation of net SurHF.

The results also indicate that the responses to C_{q1} and C_{m2} at SHL2 and GE3 are different. The C_{m2} variation has a more pronounced effect at SHL2 (Fig. 9c) while GE3 is more sensitive to C_{q1} (Fig. 9d) due to the spatial variability of meteorological forcing and LSWT over Lake Geneva. The differences in wind speed, LSWT, and relative humidity are quite noticeable between the two locations (Fig. 2; Supporting Information Fig. S6). Wind speed variations (Fig. 2b), for example, are on average higher at GE3 than at SHL2. As the value of C_{m2} mainly affects the intensity of turbulent heat fluxes at low wind regimes (Supporting Information Fig. S8a), the tendency for weak winds to occur at SHL2 reflects its sensitivity to C_{m2}. In contrast, stronger wind forcing at GE3 makes it more sensitive to the value of C_{q1}, which controls heat flux for high wind regimes (Supporting Information Fig. S8b). Again, these differences underscore the possible significant errors arising from single-point model calibration.

The same analysis can be applied to quantify the effect of geothermal heat flux on the model calibration. The water column heat content variation due to geothermal bottom heating is ~0.003 GJm^{-2}y^{-1} using the typical value for the geothermal heat flux, that is, ~0.1 Wm^{-2} (Finckh 1976),
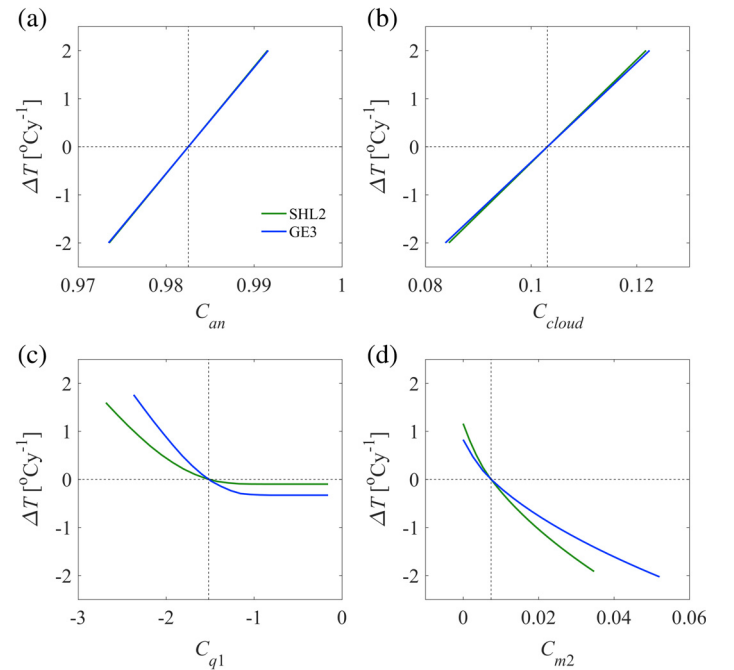

Fig. 9. Sensitivity analysis of model-induced cooling/warming for the upper 10 m of Lake Geneva at SHL2 (green lines) and GE3 (blue lines) depending on the optimum calibration factors for **(a)** C_{an}, **(b)** C_{cloud}, **(c)** C_{q1}, and **(d)** C_{m2}. The vertical dashed lines indicate the position at the optimal values for each calibration factor resulting from our analysis. It is noted that there is a high amount of overlap between the green and blue lines in panels **(a)** and **(b)**.

which is 100 times smaller than the calculated RMSE employing Model 3 (legends in Fig. 5). As this variation is small, we did not repeat the optimization procedure with the updated heat content values. Instead, we used the sensitivity analysis results to estimate its effect on the obtained calibration factors. The calculated geothermal-induced slight warming (0.003 GJm^{-2}y^{-1}) corresponds to a 0.08°Cy^{-1} variation in a 10-m water column.

Comments and recommendations

Large lakes can be characterized by considerable spatial variability in meteorological parameters. For example, the surrounding topography can exert a strong influence on the wind patterns and solar radiation, and hence on SurHF. LSWT may likewise exhibit significant spatial variability, mainly during the summertime. Therefore, the determination of SurHF at a single location only provides a partial understanding of the energy exchange dynamics over the whole lake surface and could result in significant errors in the estimation of SurHF for the whole lake. In addition, various formulations and parameterizations exist for different heat flux components, in particular for sensible and latent heat fluxes. Thus far, a systematic analysis of their optimal combination, which determines the net SurHF, was not reported. In this study, we addressed these questions by expanding the net SurHF estimation for a 7-yr period using a two-point calibration, instead of the commonly used one-point calibration. We tested 54 different net SurHF models Q_N, and presented the results for the best six models associated with different combinations of one model for solar shortwave radiation Q_{sn}, two models for atmospheric radiation Q_{an}, one model for longwave radiation from the water surface Q_{br}, and three models for turbulent heat fluxes, that is, sensible Q_{co} and latent Q_{ev} heat fluxes. For the period of 2008–2014, we evaluated the heat content response of Lake Geneva to these models by implementing frequently used coefficients given in the literature for comparable water bodies.

Our analysis emphasizes the importance of choosing appropriate calibration factors when estimating the heat budgets of large lakes. Since none of the coefficients given in the literature provided acceptable SurHF estimates, optimization was used to find the best calibration factors for the selected SurHF models. However, the common approach of computing SurHF based on a single location did not result in satisfactory SurHF predictions at both locations. We found a high sensitivity of SurHF estimations to certain calibration factors indicating that a systematic calibration of bulk models is required for each study site. We demonstrated that a small variation in calibration factors, especially those controlling atmospheric radiation, leads to a significant change in the heating/cooling estimation of the lake.

The results indicate that multipoint (two point in this study) calibration is best performed using a comprehensive model for sensible-latent heat flux calculation. The parameterization in the bulk formula based on similarity theory was found to account for the spatial variability adequately. On the other hand, the temporal variation of the air–water heat exchange is highly sensitive to the atmospheric radiation modeling. Note that all the tested models gave reasonable RMSE values for short periods, that is, < 2 yr (Fig. 6). However, only a few of them gave satisfactory calibration over two points for longer periods, that is, more than 3 yr. Therefore, an accurate model selection and calibration is important for long-term climate studies, assuming that the calibration remains valid for a shifting temperature pattern.

The results show that for the heat exchange analysis of a large lake, a properly calibrated atmospheric radiation model and, in particular, an appropriate turbulent SurHF model are essential. The quality of the results is affected by model simplifications/limitations, errors in temperature measurements and satellite data retrieval, and uncertainties associated with meteorological data. However, the results are still reliable in terms of showing the need for optimized SurHF models, the advantage of two-point versus one-point calibration, and the sensitivity of the lake heat exchange to the actual values of different calibration factors. We used a 3D numerical simulation of Lake Geneva to quantify the negligible contribution of lateral heat exchange to the heat content variation of the water column far from the shore. In general, direct measurements of different heat flux terms and advective heat transport in the water body should be carried out, as this may further refine the validation of the different SurHF terms and the heat balance algorithm applied. Likewise, measurements from more than two points would extend and enhance the present survey. The methodology developed in this study and the results obtained improve the computation of the spatio-temporal SurHF over large lakes and consequently give a better estimation of the total energy exchange at the air–water interface. At the same time, these results may increase the reliability of numerical weather modeling by better accounting for lake-atmosphere heat exchanges.

References

Akitomo, K., M. Kurogi, and M. Kumagai. 2004. Numerical study of a thermally induced gyre system in Lake Biwa. Limnology **5**: 103–114. doi:10.1007/s10201-004-0122-9

Anderson, E. J., and D. J. Schwab. 2017. Meteorological influence on summertime baroclinic exchange in the straits of Mackinac. J. Geophys. Res.: Oceans **122**: 2171–2182. doi:10.1002/2016JC012255

Arvola, L., et al. 2010. The impact of the changing climate on the thermal characteristics of lakes, p. 85–101. *In* G. George [ed.]The impact of climate change on European Lakes. Springer. doi:10.1007/978-90-481-2945-4_6

Austin, J. A., and J. Allen. 2011. Sensitivity of summer Lake Superior thermal structure to meteorological forcing. Limnol. Oceanogr. **56**: 1141–1154. doi:10.4319/lo.2011.56.3.1141

Babanin, A. V., and V. K. Makin. 2008. Effects of wind trend and gustiness on the sea drag: Lake George study. J. Geophys. Res.: Oceans **113**: C02015. doi:10.1029/2007jc004233

Beletsky, D., J. H. Saylor, and D. J. Schwab. 1999. Mean circulation in the Great Lakes. J. Great Lakes Res. **25**: 78–93. doi:10.1016/S0380-1330(99)70718-5

Beletsky, D., and D. J. Schwab. 2008. Climatological circulation in Lake Michigan. Geophys. Res. Lett. **35**: L21604. doi:10.1029/2008gl035773

Bennington, V., G. A. McKinley, N. Kimura, and C. H. Wu. 2010. General circulation of Lake Superior: Mean, variability, and trends from 1979 to 2006. J. Geophys. Res.: Oceans **115**: C12015. doi:10.1029/2010jc006261

Beven, K., and A. Binley. 1992. The future of distributed models: Model calibration and uncertainty prediction. Hydrol. Proc. **6**: 279–298. doi:10.1002/hyp.3360060305

Bonvin, F., A. M. Razmi, D. A. Barry, and T. Kohn. 2013. Micropollutant dynamics in Vidy Bay- A coupled hydrodynamic-photolysis model to assess the spatial extent of ecotoxicological risk. Environ. Sci. Technol. **47**: 9207–9216. doi:10.1021/es401294c

Bourassa, M. A., D. G. Vincent, and W. L. Wood. 1999. A flux parameterization including the effects of capillary waves and sea state. J. Atmos. Sci. **56**: 1123–1139. doi:10.1175/1520-0469(1999)056<1123:Afpite>2.0.Co;2

Bowen, I. S. 1926. The ratio of heat losses by conduction and by evaporation from any water surface. Phys. Rev. **27**: 779–787. doi:10.1103/Physrev.27.779

Boyce, F. M., M. A. Donelan, P. F. Hamblin, C. R. Murthy, and T. J. Simons. 1989. Thermal structure and circulation in the Great Lakes. Atmos.-Ocean **27**: 607–642. doi:10.1080/07055900.1989.9649358

Bradley, E. F., P. A. Coppin, and J. S. Godfrey. 1991. Measurements of sensible and latent heat flux in the western equatorial Pacific Ocean. J. Geophys. Res.: Oceans **96**: 3375–3389. doi:10.1029/90JC01933

Brutsaert, W. 1975. Derivable formula for long-wave radiation from clear skies. Water Resour. Res. **11**: 742–744. doi:10.1029/Wr011i005p00742

Carmack, E. C. 1979. Combined influence of inflow and lake temperatures on spring circulation in a riverine lake. J. Phys. Oceanogr. **9**: 422–434. doi:10.1175/1520-0485(1979)009<0422:Cioial>2.0.Co;2

Charnock, H. 1955. Wind stress on a water surface. Q. J. Roy. Meteor. Soc. **81**: 639–640. doi:10.1002/qj.49708135027

Churchill, J. H., and W. Charles Kerfoot. 2007. The impact of surface heat flux and wind on thermal stratification in portage Lake, Michigan. J. Great Lakes Res. **33**: 143–155. doi:10.3394/0380-1330(2007)33[143,TIOSHF]2.0.CO;2

Cogley, J. G. 1979. Albedo of water as a function of latitude. Mon. Weather Rev. **107**: 775–781. doi:10.1175/1520-0493(1979)107<0775:Taowaa>2.0.Co;2

Crawford, T. M., and C. E. Duchon. 1999. An improved parameterization for estimating effective atmospheric emissivity for use in calculating daytime downwelling longwave radiation. J. Appl. Meteorol. **38**: 474–480. doi:10.1175/1520-0450(1999)038<0474:Aipfee>2.0.Co;2

Davies, J. A., P. J. Robinson, and M. Nunez. 1971. Field determinations of surface emissivity and temperature for Lake Ontario. J. Appl. Meteorol. **10**: 811–819. doi:10.1175/1520-0450(1971)010<0811:FDOSEA>2.0.CO;2

Deardorff, J. W. 1968. Dependence of air-sea transfer coefficients on bulk stability. J. Geophys. Res. **73**: 2549–2557. doi:10.1029/JB073i008p02549

Derecki, J. A. 1976. Heat storage and advection in Lake Erie. Water Resour. Res. **12**: 1144–1150. doi:10.1029/Wr012i006p01144

Dommenget, D., and M. Rezny. 2018. A caveat note on tuning in the development of coupled climate models. J. Adv. Model. Earth Syst. **10**: 78–97. doi:10.1002/2017MS000947

Emery, K. O., and G. T. Csanady. 1973. Surface circulation of lakes and nearly land-locked seas. Proc. Natl. Acad. Sci. U. S. A. **70**: 93–97. doi:10.1073/Pnas.70.1.93

Fairall, C. W., E. F. Bradley, D. P. Rogers, J. B. Edson, and G. S. Young. 1996. Bulk parameterization of air-sea fluxes for Tropical Ocean global atmosphere coupled ocean atmosphere response experiment. J. Geophys. Res.: Oceans **101**: 3747–3764. doi:10.1029/95jc03205

Finckh, P. 1976. Wärmeflussmessungen in Randalpenseen. Dissertation No. 5787. ETH Zürich, Switzerland. doi:10.3929/ethz-a-000101336

Fink, G., M. Schmid, B. Wahl, T. Wolf, and A. Wüest. 2014. Heat flux modifications related to climate-induced warming of large European lakes. Water Resour. Res. **50**: 2072–2085. doi:10.1002/2013wr014448

Finlay, K., R. J. Vogt, M. J. Bogard, B. Wissel, B. M. Tutolo, G. L. Simpson, and P. R. Leavitt. 2015. Decrease in CO_2 efflux from northern hardwater lakes with increasing atmospheric warming. Nature **519**: 215–218. doi:10.1038/nature14172

Fritsch, F. N., and R. E. Carlson. 1980. Monotone piecewise cubic interpolation. Siam. J. Numer. Anal. **17**: 238–246. doi:10.1137/0717021

Geernaert, G. L., K. L. Davidson, S. E. Larsen, and T. Mikkelsen. 1988. Wind stress measurements during the Tower Ocean wave and radar dependence experiment. J. Geophys. Res.: Oceans **93**: 13913–13923. doi:10.1029/Jc093ic11p13913

Gill, A. E. 1982. Atmosphere-ocean dynamics. Academic Press. doi:10.1002/qj.49711046322

Gillet, C., and P. Quetin. 2006. Effect of temperature changes on the reproductive cycle of roach in Lake Geneva from 1983 to 2001. J. Fish Biol. **69**: 518–534. doi:10.1111/j.1095-8649.2006.01123.x

Graf, W. H., and J. P. Prost. 1980. Aerodynamic drag and its relation to the sea state: With data from Lake Geneva. Arch. Meteorol. Geophy. A. **29**: 67–87. doi:10.1007/Bf02247734

Heikinheimo, M., M. Kangas, T. Tourula, A. Venalainen, and S. Tattari. 1999. Momentum and heat fluxes over lakes

Tamnaren and Raksjo determined by the bulk-aerodynamic and eddy-correlation methods. Agric. For. Meteorol. **98-9**: 521–534. doi:10.1016/S0168-1923(99)00121-5

Henderson-Sellers, B. 1986. Calculating the surface energy balance for lake and reservoir modeling: A review. Rev. Geophys. **24**: 625–649. doi:10.1029/Rg024i003p00625

Jin, W. 1994. The sea-surface is aerodynamically rough even under light winds. Bound.-Lay. Meteor. **69**: 149–158. doi:10.1007/BF00713300

Koch, S. E., M. Desjardins, and P. J. Kocin. 1983. An interactive Barnes objective map analysis scheme for use with satellite and conventional data. J. Clim. Appl. Meteorol. **22**: 1487–1503. doi:10.1175/1520-0450(1983)022<1487:Aiboma>2.0.Co;2

Kuhn, V. W. 1978. Aus Wärmehaushalt und Klimadaten berechnete Verdunstung des Zürichsees. Vjschr. Naturf. Ges. Zürich **123**: 261–283. http://www.ngzh.ch/publikationen/vjs/123/4 (last accessed 5 July 2018).

Laird, N. F., and D. A. R. Kristovich. 2002. Variations of sensible and latent heat fluxes from a Great Lakes buoy and associated synoptic weather patterns. J. Hydrometeorol. **3**: 3–12. doi:10.1175/1525-7541(2002)003<0003:Vosalh>2.0.Co;2

Lemmin, U., and N. D'Adamo. 1996. Summertime winds and direct cyclonic circulation: Observations from Lake Geneva. Ann. Geophys., Ser. A **14**: 1207–1220. doi:10.1007/s005850050384

Lenters, J. D., T. K. Kratz, and C. J. Bowser. 2005. Effects of climate variability on Lake evaporation: Results from a long-term energy budget study of Sparkling Lake, northern Wisconsin (USA). J. Hydrol. **308**: 168–195. doi:10.1016/j.jhydrol.2004.10.028

Lin, W. Q., L. P. Sanford, S. E. Suttles, and R. Valigura. 2002. Drag coefficients with fetch-limited wind waves. J. Phys. Oceanogr. **32**: 3058–3074. doi:10.1175/1520-0485(2002)032<3058:Dcwflw>2.0.Co;2

Liston, G. E., and K. Elder. 2006. A meteorological distribution system for high-resolution terrestrial modeling (MicroMet). J. Hydrometeorol. **7**: 217–234. doi:10.1175/Jhm486.1

Livingstone, D. M., and D. M. Imboden. 1989. Annual heat balance and equilibrium temperature of Lake Aegeri. Switzerland. Aquat. Sci. **51**: 351–369. doi:10.1007/Bf00877177

Lofgren, B. M., and Y. C. Zhu. 2000. Surface energy fluxes on the Great Lakes based on satellite-observed surface temperatures 1992 to 1995. J. Great Lakes Res. **26**: 305–314. doi:10.1016/S0380-1330(00)70694-0

MacIntyre, S., J. R. Romero, and G. W. Kling. 2002. Spatial-temporal variability in surface layer deepening and lateral advection in an embayment of Lake Victoria, East Africa. Limnol. Oceanogr. **47**: 656–671. doi:10.4319/lo.2002.47.3.0656

Mahrt, L., D. Vickers, J. Howell, J. Hojstrup, J. M. Wilczak, J. Edson, and J. Hare. 1996. Sea surface drag coefficients in the Riso Air Sea experiment. J. Geophys. Res.: Oceans **101**: 14327–14335. doi:10.1029/96jc00748

Merzi, N., and W. H. Graf. 1988. Wind stress over water waves: Field experiments on Lake of Geneva. Meteorol. Atm. Phys. **39**: 14–24. doi:10.1007/Bf01029894

Mironov, D. V. 2008. Parameterization of lakes in numerical weather prediction: Description of a lake model. COSMO technical report, **11**: 1–44. http://www.cosmo-model.org/content/model/documentation/techReports/docs/techReport11.pdf (last accessed 5 July 2018).

Momii, K., and Y. Ito. 2008. Heat budget estimates for Lake Ikeda. Jpn. J. Hydrol. **361**: 362–370. doi:10.1016/j.jhydrol.2008.08.004

Monin, A. S., and A. M. Obukhov. 1954. Basic laws of turbulent mixing in the ground layer of the atmosphere. Tr. Akad. Nauk SSSR Geofiz. Inst. **24**: 163–187.

Moukomla, S., and P. D. Blanken. 2017. The estimation of the north American Great Lakes turbulent fluxes using satellite remote sensing and MERRA reanalysis data. Remote Sens. (Basel) **9**: 141. doi:10.3390/Rs9020141

Murakami, M., Y. Oonishi, and H. Kunishi. 1985. A numerical simulation of the distribution of water temperature and salinity in the Seto Inland Sea. J. Oceanogr. Soc. Jpn **41**: 213–224. doi:10.1007/BF02109271

Nordbo, A., S. Launiainen, I. Mammarella, M. Lepparanta, J. Huotari, A. Ojala, and T. Vesala. 2011. Long-term energy flux measurements and energy balance over a small boreal lake using eddy covariance technique. J. Geophys. Res.: Atmos. **116**: D02119. doi:10.1029/2010jd014542

Nussboim, S., A. Rimmer, Y. Lechinsky, P.-O. Gutman, and D. Broday. 2017. Improving the estimation of Lake Kinneret's heat balance and surface fluxes using the Kalman filter algorithm. Limnol. Oceanogr.: Methods **15**: 467–479. doi:10.1002/lom3.10173

Octavio, K. A. H. 1977. Vertical heat transport mechanisms in lakes and reservoirs. Thesis, Ralph M. Parsons Laboratory for Water Resources and Hydrodynamics. Mass. Inst. Tech., Cambridge, Massachusetts, USA. Available from http://hdl.handle.net/1721.1/52844 (last accessed 5 July 2018).

Oesch, D. C., J. M. Jaquet, A. Hauser, and S. Wunderle. 2005. Lake surface water temperature retrieval using advanced very high resolution radiometer and moderate resolution imaging Spectroradiometer data: Validation and feasibility study. J. Geophys. Res.: Oceans **110**: C12014. doi:10.1029/2004jc002857

Riffler, M., G. Lieberherr, and S. Wunderle. 2015. Lake surface water temperatures of European alpine lakes (1989-2013) based on the advanced very high resolution radiometer (AVHRR) 1 km data set. Earth Sys. Sci. Data **7**: 1–17. doi:10.5194/essd-7-1-2015

Rimmer, A., R. Samuels, and Y. Lechinsky. 2009. A comprehensive study across methods and time scales to estimate surface fluxes from Lake Kinneret. Israel. J. Hydrol. **379**: 181–192. doi:10.1016/j.jhydrol.2009.10.007

Rouse, W. R., P. D. Blanken, N. Bussieres, C. J. Oswald, W. M. Schertzer, C. Spence, and A. E. Walker. 2008. Investigation of the thermal and energy balance regimes of Great Slave and Great Bear Lakes. J. Hydrometeorol. **9**: 1318–1333. doi:10.1175/2008JHM977.1

Rouse, W. R., C. M. Oswald, J. Binyamin, P. D. Blanken, W. M. Schertzer, and C. Spence. 2003. Interannual and seasonal variability of the surface energy balance and temperature of Central Great Slave Lake. J. Hydrometeorol. **4**: 720–730. doi:10.1175/1525-7541(2003)004<0720:Iasvot>2.0.Co;2

Ryan, P. J., D. R. F. Harleman, and K. D. Stolzenbach. 1974. Surface heat loss from cooling ponds. Water Resour. Res. **10**: 930–938. doi:10.1029/Wr010i005p00930

Satterlund, D. R. 1979. An improved equation for estimating long-wave-radiation from the atmosphere. Water Resour. Res. **15**: 1649–1650. doi:10.1029/Wr015i006p01649

Schertzer, W. M. 1978. Energy budget and monthly evaporation estimates for Lake Superior, 1973. J. Great Lakes Res. **4**: 320–330. doi:10.1016/S0380-1330(78)72201-X

Simon, A. 1997. Turbulent mixing in the surface boundary layer of lakes. Dissertation No. 12272. ETH Zürich, Switzerland. doi: 10.3929/ethz-a-001843543

Simons, T. J. 1980. Circulation models of lakes and inland seas. Bulletin 203. Canadian Bulletin of Fisheries and Aquatic Sciences, Department of Fisheries and Oceans, Ottawa, Ont. Canada. 146 pp.

Spence, C., P. D. Blanken, N. Hedstrom, V. Fortin, and H. Wilson. 2011. Evaporation from Lake Superior: 2-spatial distribution and variability. J. Great Lakes Res. **37**: 717–724. doi:10.1016/j.jglr.2011.08.013

Stepanenko, V., K. D. Johnk, E. Machulskaya, M. Perroud, Z. Subin, A. Nordbo, I. Mammarella, and D. Mironov. 2014. Simulation of surface energy fluxes and stratification of a small boreal lake by a set of one-dimensional models. Tellus, Ser. A. **66**: 21389. doi:10.3402/Tellusa.V66.21389

Sweers, H. E. 1976. Nomogram to estimate heat exchange coefficient at air-water interface as a function of wind speed and temperature: Critical survey of some literature. J. Hydrol. **30**: 375–401. doi:10.1016/0022-1694(76)90120-7

Tanentzap, A. J., D. P. Hamilton, and N. D. Yan. 2007. Calibrating the dynamic reservoir simulation model (DYRESM) and filling required data gaps for one-dimensional thermal profile predictions in a boreal lake. Limnol. Oceanogr.: Methods **5**: 484–494. doi:10.4319/lom.2007.5.484

Taylor, K. E. 2001. Summarizing multiple aspects of model performance in a single diagram. J. Geophys. Res.: Atmos. **106**: 7183–7192. doi:10.1029/2000jd900719

Thiery, W., A. Martynov, F. Darchambeau, J. P. Descy, P. D. Plisnier, L. Sushama, and N. P. M. van Lipzig. 2014a. Understanding the performance of the FLake model over two African Great Lakes. Geosci. Model Dev. **7**: 317–337. doi:10.5194/gmd-7-317-2014

Thiery, W., et al. 2014b. LakeMIP Kivu: Evaluating the representation of a large, deep tropical lake by a set of one-dimensional lake models. Tellus, Ser. A. **66**: 21390. doi: 10.3402/Tellusa.V66.21390

Toffoli, A., L. Loffredo, P. Le Roy, J. M. Lefevre, and A. V. Babanin. 2012. On the variability of sea drag in finite water

depth. J. Geophys. Res.: Oceans **117**: C00J25. doi:10.1029/2011jc007857

Van Emmerik, T. H. M., A. Rimmer, Y. Lechinsky, K. J. R. Wenker, S. Nussboim, and N. C. van de Giesen. 2013. Measuring heat balance residual at lake surface using distributed temperature sensing. Limnol. Oceanogr.: Methods **11**: 79–90. doi:10.4319/lom.2013.11.79

Verburg, P., and J. P. Antenucci. 2010. Persistent unstable atmospheric boundary layer enhances sensible and latent heat loss in a tropical great lake: Lake Tanganyika. J. Geophys. Res.: Atmos. **115**: D11109. doi:10.1029/2009jd012839

Wahl, B., and F. Peeters. 2014. Effect of climatic changes on stratification and deep-water renewal in Lake Constance assessed by sensitivity studies with a 3D hydrodynamic model. Limnol. Oceanogr. **59**: 1035–1052. doi:10.4319/lo.2014.59.3.1035

Wang, W., et al. 2014. Temporal and spatial variations in radiation and energy balance across a large freshwater lake in China. J. Hydrol. **511**: 811–824. doi:10.1016/j.jhydrol.2014.02.012

Webster, P. J., and R. Lukas. 1992. Toga Coare: The coupled ocean-atmosphere response experiment. B. Am. Meteorol. Soc. **73**: 1377–1416. doi:10.1175/1520-0477(1992)073<1377:Tctcor>2.0.Co;2

Wei, Z. W., A. Miyano, and M. Sugita. 2016. Drag and bulk transfer coefficients over water surfaces in light winds. Bound.-Lay. Meteor. **160**: 319–346. doi:10.1007/s10546-016-0147-8

Woolway, R. I., I. D. Jones, H. Feuchtmayr, and S. C. Maberly. 2015a. A comparison of the diel variability in epilimnetic temperature for five lakes in the English Lake District. Inland Waters **5**: 139–154. doi:10.5268/Iw-5.2.748

Woolway, R. I., I. D. Jones, D. P. Hamilton, S. C. Maberly, K. Muraoka, J. S. Read, R. L. Smyth, and L. A. Winslow. 2015b. Automated calculation of surface energy fluxes with high-frequency lake buoy data. Environ. Model. Software **70**: 191–198. doi:10.1016/j.envsoft.2015.04.013

Wüest, A., and A. Lorke. 2003. Small-scale hydrodynamics in lakes. Ann. Rev. Fluid Mech. **35**: 373–412. doi:10.1146/annurev.fluid.35.101101.161220

Xiao, W., S. D. Liu, W. Wang, D. Yang, J. P. Xu, C. Cao, H. C. Li, and X. H. Lee. 2013. Transfer coefficients of momentum, heat and water vapour in the atmospheric surface layer of a large freshwater lake. Bound.-Lay. Meteor. **148**: 479–494. doi:10.1007/s10546-013-9827-9

Xue, P. F., D. J. Schwab, and S. Hu. 2015. An investigation of the thermal response to meteorological forcing in a hydrodynamic model of Lake Superior. J. Geophys. Res.: Oceans **120**: 5233–5253. doi:10.1002/2015JC010740

Yang, J., Z.-H. Wang, Q. Li, N. Vercauteren, E. Bou-Zeid, and M. B. Parlange. 2017. A novel approach for unraveling the energy balance of water surfaces with a single depth temperature measurement. Limnol. Oceanogr. **62**: 89–103. doi:10.1002/lno.10378

Zeng, X. B., M. Zhao, and R. E. Dickinson. 1998. Intercomparison of bulk aerodynamic algorithms for the computation of sea surface fluxes using TOGA COARE and TAO data. J. Climate **11**: 2628–2644. doi:10.1175/1520-0442(1998)011<2628:Iobaaf>2.0.Co;2

Zhu, J. R., C. S. Chen, E. Ralph, S. A. Green, J. W. Budd, and F. Y. Zhang. 2001. Prognostic modeling studies of the Keweenaw current in Lake Superior. Part II: Simulation. J. Phys. Oceanogr. **31:** 396-410. doi:10.1175/1520-0485(2001)031<0396:Pmsotk>2.0.Co;2.